MINIaturized JOINT structures and 3D-living microfluidics to study cartilage degenerative diseases

MINI-JOINT

Major Internship report

Universiteit Utrecht

Author: Núria Ginés Rodriguez

Student number: 6526543

Date: 8th December 2021

First Examiner: Riccardo Levato

Second Examiner: Yang Li

INDEX

ABSTRACT

In recent years, advances in fabrication techniques and 3D printing have allowed development in advanced in-vitro models as bioreactors. 3D bioprinting enables the manufacturing of complex and intricate architectures that have been unprecedented until recently. Their deployment tailors designs and prototypes while integrating cell culture and hydrogel development in micro-perfused platforms. These novel platforms allow the establishment and perfusion of 3D bioprinted cellular scaffolds, which have proven to be more efficient in tissue engineering than traditional 2D cell culture. 3D scaffolds tend to derive from hydrogels, which are highly tuneable, natural or synthetic water-based matrixes that allow for functionalization with extracellular matrix-like molecules and cues. Physiologic microenvironments are highly complex, cell-cell and cell-matrix interactions maintain homeostasis in native tissue. When homeostatic interactions are lost, the microenvironment shifts to a diseased state. To cure a disease, it is important to understand the intricate complexity of these microenvironments. In-vitro models try to recapitulate physiologic microenvironments to better understand the disease progression and how to restore the healthy state.
In this project, biofabrication and tissue engineering techniques are combined to advance the field of bioreactor-like *in-vitro* models for inflammatory diseases of the knee joint environment. Volumetric bioprinting is a novel 3D printing technique, here optimized for BM-hMSC scaffolds for trabecular bone. Candidate materials for the osteochondral interface are assayed. A two-chamber bioreactor is custom designed and assembled to perfuse a bone and a cartilage compartment independently with an engineered osteochondral interface as a physical barrier.

LAYMAN SUMMARY

The interactions between cells and the microenvironment determine whether a tissue maintains homeostasis. The performance of tissues is affected by minute changes in the architecture, composition or signalling. The disease is associated with a deviation from the healthy state. Thus, it is of paramount importance to understand the characteristics of the healthy state before understanding or resolving the pathways leading to disease. I*n-vitro* models strive to replicate the physiologic microenvironments in the laboratory. These models allow for limited reproduction of a certain tissue. *In-vitro* models aim to understand the interplay leading to homeostasis or disease. In-vitro models have different levels of complexity, from simple 2D cell culture to study the cell-cell interaction under the influence of a myriad of molecules and drugs to more complex bioreactors or micro perfused systems as organs-on-chip. Each increase in the model's complexity results in a better mimic of the physiologic state. From cell-cell interactions to patterning and functionalization of scaffolding materials. Multi tissue systems and hydrogel patterning of diverse cell types. In recent years, Biofabrication techniques have allowed to increase the complexity of *in-vitro* models. Biofabrication is the positioning and spacing of materials in a particular order to achieve certain shapes and objects determined by a computer-generated design. Advances in Biofabrication and tissue engineering allow combining complex cellular architectures with supporting materials and deliver nutrients, growth factors and molecules. The project focuses on developing a bioreactor model of the knee joint environment. Inflammatory diseases are a leading cause of disability and morbidity. In 2016, Knee Osteoarthritis affected 15.6% of men and 30.5% of women aged 55 and over. KOA is a chronic disease the only treatments are symptom management and total knee joint replacement. It is important to develop models to understand the processes of KOA development and assay prospective future therapies.

This project combines advances in fabrication and tissue engineering techniques to achieve a bioreactor platform where two different compartments can be simultaneous and independently perfused with bone and cartilage media. The project develops the novel Volumetric Bioprinting technology for the Biofabrication of BM-hMSC scaffolds for trabecular bone engineering. Furthermore, the osteochondral interface is engineered from diverse candidate materials. The project culminates in the development of a dually perfused bioreactor platform to integrate four different tissue types, bone, osteochondral interface, cartilage and a synovial lining. The bioreactor has proven to be leakproof at the interfaces between the platform's components and between the compartments.

The development of the bioreactor model is an advance to achieve a medically relevant in-vitro model for the study of the interplay in the knee joint environment both in states of health and disease.

INTRODUCTION

Osteoarthritis (OA) is a degenerative joint disease seen in larger synovial joints. In developed countries, OA is highly prevalent among the elderly. In 2016, 1.25 million patients in the Netherlands alone were living with OA diagnoses[1]. From those 1.25 million Dutch patients, the majority suffer from OA affecting the knee joint, Knee Osteoarthritis (KOA), which prevalence is 15,6% in men and up to 30,5% in women over 55 years of age[2]. Nevertheless, not all cases are symptomatic. Only 15% of patients with radiographic evidence of cartilage degeneration will develop KOA symptoms[3]. The hallmark of KOA is cartilage degeneration that expands to other structures in the joint, followed by extensive pain and eventual loss of function of the knee[2]. It is the largest synovial joint in the human body composed of several distinct tissues: bone, hyaline cartilage, ligaments, tendons, menisci and a synovial membrane. Hyaline cartilage is an avascular and non-innervated structure with low regenerative capacity, the first tissue to be affected by OA. Due to the lack of nerve terminations in the hyaline cartilage, KOA will not be symptomatic until damage has spread to other innervated tissues[4]. The surrounding structures prone to damage are the synovium, subchondral bone, ligaments, meniscus and neighbouring musculature[5]. The most common afflictions found in large synovial joints are inflammatory such as osteoarthritis or rheumatoid arthritis (RA)[6]. These diseases are chronic and degenerative. They account for irreversible malformations to the joint cavity that progress and worsen over time[7]. Alterations to any of the knee joint components will affect the neighbouring structures, suggesting the importance of cross-talk in maintaining homeostasis[8]. OA and RA are degenerative diseases with high prevalence among population aged 50 or over. Symptoms effect patients' quality of life and impose a high economic burden on healthcare. There is no cure for inflammatory diseases of the synovial joints. The only available treatments are symptom management and eventual total knee joint replacement. Novel curative therapies for inflammatory diseases are needed. The development of new curative therapies is hampered by a lack of relevant in-vitro models. To understand how OA affects the joint capsule in the knee and achieve a reliable *in-vitro* model some target tissues need to be selected. Previous studies have determined that the most relevant tissues involved in inflammatory diseases are hyaline cartilage and subchondral bone. Several studies have indicated that the osteochondral interface is also involved in the progression of inflammatory symptoms. Thus, the project will focus on trabecular bone, hyaline cartilage and osteochondral interface.

Trabecular bone is a subset of bone tissue found at the end of long bones it transfers load from the joint capsule to the cortex of the bone[25]. To promote mineralization of engineered bone constructs, some studies have supplemented hydrogels as gelatine or gelatine methacrylate (GelMa) with peptides or calcium phosphate-containing materials[26]. The load-bearing and load distribution properties of trabecular bone are a result of its intricate architecture. Factors as porosity, pore network and interconnectivity have a role in the properties of engineered bone tissue. Porosity allows cells to migrate, colonize and divide in the bone scaffold. An interconnected pore network enables cell mobility and permeability of the construct. Too porous scaffolds can be mechanically weak and compromise the bone's load bearing function[27]. A compromise is needed between porosity and mechanical properties when engineering bone constructs[28]. Many literature references describe the use of Mesenchymal Stem Cells (MSCs) as a candidate cell source for the engineering of trabecular bone. MSCs are relatively easy to harvest from patient samples as bone marrow or adipose tissue, with bone-marrow-derived MSCs (BM-MSCs) being the most frequently used cell source in bone tissue engineering[29]. BM-MSCs can be expanded in vitro while maintaining their stem cell phenotype, then differentiated *in-vitro*[29, 30].

Hyaline cartilage prevents erosion by contact between two bones' ends and distributes the load from the joint capsule to the subchondral bone[31]. Due to the load-distributing function, the tissue is under constant load. Hyaline cartilage is an avascular, non-innervated, scarcely cellular tissue with little regenerative capacity[33]. The ECM is primarily composed of collagen type II, proteoglycans and glycosaminoglycans produced by chondrocytes, the main cell population. Chondrocytes account for 5-10% of the tissue. *In-vitro* expansion of

cartilaginous tissue is difficult. Chondrocytes exhibit large degrees of dedifferentiation and phenotypic changes altering the production of ECM molecules as the shift in collagen secretion from type II to type I[32]. Hyaline cartilage has several layers of transition between its attachment to the bone to the surface in contact with the synovial fluid. The first cartilage layer in contact with the trabecular bone is known as calcified cartilage, or osteochondral interface, which is 50 – 250 µm thick. It maintains the structural integrity of the osteochondral unit during load of the joint as walking, jumping etc. During movement, the tensile, compressive and shear forces are transmitted from the upper surface of the cartilage layer to the mineralized bone[34]. The interface is a combination of ECM secreted from bone and cartilage, the structure develops from articular cartilage, which is calcified by the invasion of collagen type I fibres from the osteoblasts present in the ends of long bones and is scarcely cellularized[35]. The calcified cartilage layer is semi-permeable and allows the diffusion of small molecules of up to 2000 Da from bone to cartilage[36]. The osteochondral interface thickens when affected by inflammatory diseases, reducing the permeability to small molecules[37]. In a study by Pouran et al., the permeability of the interface was measured in both healthy and diseased osteochondral units and differences in permeability between health and diseased states were found. Suggesting that the osteochondral interface plays an important role in the development of inflammatory diseases of the knee[38].

In-vitro models are platforms that recapitulate the function or architecture of a specific tissue, organ or conjunction of tissues. Many different approaches have been developed, from 2D cell cultures to microfluidics and organs on chip[6]. In-vitro models and animal studies are part of drug development during pre-clinical trials. Animal models allow for the screening of drug candidates in complex environments. Pre-clinical testing determines whether a drug candidate is safe to use in human trials[9 10]. The most used and already established in-vitro models use panels and arrays of cells cultured in 2D, tissue explants, scaffolds and 3D environments to recreate the in-human state. Animal models are used to study the microenvironment on a bigger scale as an organ, barrier system or metabolic pathway. These models fail to reproduce the intrinsic complexity of organ systems, account for species-specific differences or lack resemblance to native human physiology[11]. This lack of translation leads to drugs being deemed as safe or effective until advanced stages of clinical trials, where they fail due to faulty preclinical models. There is a lack of resemblance between pre-clinical models and the complex interaction found in healthy and diseased human tissues.

As the complexity of in-vitro models increases, the closer research is to decipher complex physiologic processes. In-vitro models offer a simplified approach, the isolation of a complex environment to study the characteristics of health and disease[12]. There have been many in-vitro models proposed for the knee joint environment, each with its advantages and drawbacks, the most common approaches for in-vitro models of synovial joints are described in table 1.

Method	Advantage	Limitation
2D monolayers[13]	Allow high throughput screening. Simple to establish and maintain. Study response of cells to contact with factors or complex formulations.	When isolated cells are prone to change phenotype. Lack crosstalk of other cells and ECM. Challenge cell source selection. Not representative of complex environment.
3D scaffolds[14]	Hydrogels can mimic ECM. Factors can be provided. Different cell types can be combined in a 3D architecture. Study of matrix-cell and cell-cell interactions.	Normally cultured under static conditions. Lacks influence of neighbouring tissues. Absence of tissue substrates.

Tissue explants[15, 16] (cadaveric or living donors)	Cells cultured in their natural microenvironment. Allows to study the environment and how it responds to changes: mechanic load, inflammation, erosion, disease.	High variability between donors leads to low reproducibility. Explants degrade and decompose over time, phenotypes can change. Low availability of human explants
Bioreactors[17, 18]	Controlled culture environment. Culture of explants, cells, engineered tissues and factor addition. Semi-dynamic conditions.	Lack of tissue-tissue interface. Lack of gas and molecular gradients. Some models lack mechanical stimuli.
Organs-on-chip[19]	Multiple cell types. Engineered micro perfused chambers. High control of the cell architecture. Recapitulate an organ/tissue microenvironment which can be monitored in real time.	Low to medium throughput. High complexity of the systems.

3D culture in hydrogel scaffolds solves some of the shortcomings of 2D cell cultures. Hydrogels are polymeric networks with high tunability that allow mimicking tissue environments[20 21]. Once cells and biological molecules are added to a hydrogel formulation, the obtained biomaterial is known as bioink[22]. ECM-derived hydrogels allow for the incorporation of signalling molecules that regulate cell migration, invasion and proliferation among others[23]. Hydrogels have highly tuneable structures that allow engineering biocompatible materials with different properties and biologic functionalization[24 25]. The development of 3D fabrication techniques has allowed advances in 3D *in-vitro* models. Biofabrication, or 3D bioprinting, is a rising field that holds the potential to generate constructs that recapitulate the complexity of native tissues and organs. Groll et al. (2016) defined Biofabrication as "the automated generation of biologically functional products with structural organization. From living cells, bioactive molecules, biomaterials, cell aggregates, or hybrid cell-material constructs through bioprinting, or bioassembly, and subsequent tissue maturation process."[26 22]. Biofabrication achieves resemblance to native tissue through spatial patterning or deposition of cells and molecules in concrete locations of a 3D space. Advances in imaging techniques and computer-aided design (CAD) software are used to guide a printer through the working space where cells and materials are continuously, or discontinuously deposited in a 3D space[27 26]. With a combination of tools, improved models can better recapitulate physiologic function. A 3D scaffold allows studying the cell-cell and cell-material interactions in a structure that resembles the native environment more than a 2D culture. Furthermore, cells maintain a better native phenotype in tissue-like structures. Nevertheless, 3D scaffolds also have drawbacks in recapitulating the complex microenvironment *in-vitro.* These models generally lack mechanical cues, tend to be cultured in static conditions and lack the influence of neighbouring tissues[14]. Bioreactors are closed systems where a 3D scaffold or tissue explant is cultured under dynamic conditions and can apply mechanical cues to the neo-tissue[18]. As an example of the application of bioreactors, C. Meinert et al. designed a bioreactor for biaxial mechanical loading of cartilage scaffolds. Their setup allowed different types of mechanical load to the cartilage constructs, which demonstrated that certain types of mechanical loading enhanced the biosynthetic activity of chondrocytes embedded in the scaffold[28]. In another example by A. Takeri et al., a bioreactor to mimic the load conditions of the cartilage in synovial joints is developed to study the effect of load and environmental cues on engineering and culture of cartilage *in-vitro*. A cartilage scaffold is cultured in a box with controlled environmental conditions and subjected to a typical loading pattern seen

in the knee joint[18]. Thus bioreactors improve the culture conditions seen in 3D scaffolds. Another novel approach to optimize *in-vitro* models is organs-on-chip. Organs on a chip are reverse-engineered microsystems, they allow for the combination of spatially patterned hydrogels, cell culture and micro-perfusion of nutrients and biologically relevant factors. Organs-on-chip can be established for single organs or connect multiple organic micro-systems with appropriate perfusion setups[19]. Organs-on-chip is a simplified structure that allows the reproduction of variable degrees of tissue complexity. Their ease of manipulation and high resemblance to the physiologic environment has attracted interest in organs-on-chip as improved *in-vitro* models to study health and disease. Few organs-on-chip platforms have been developed for the synovial joint or specifically for the knee joint. Some examples in literature describe the establishment of organs-on-chip for different tissues found in the knee, bone, cartilage and osteochondral unit. J.S. Jeon et al., establish a vascularized bone-on-chip to study breast cancer metastases to bone tissue[29]. The establishment of the micro-fluidic platform was successful and saw microvascular network formation in 4 days of culture. Which cannot be reproduced in a 3D scaffold approach with a short culture time. Another study by R. Kamm et al., established a bone metastasis-on-chip platform with three different channels, endothelial, bone cancer and healthy bone that used a dialysis membrane to separate the compartments[30]. There, they observed invasion of cancerous cells and blood vessel formation in the cancer compartment. C. Paggi et al., describe the assembly of a three-layered cartilage-on-chip platform. Their platform includes mechanical stimulation to a micro perfused agarose gel laden with differentiated human chondrocytes. The platform allows the study of cell behaviour under different mechanical loads in a section of healthy or diseased cartilage[31]. P. Orcchetta et al., designed an on-chip platform to study the onset of OA in articular cartilage. In their design, an articular cartilage hydrogel from polyethylene glycol (PEG) laden with human chondrocytes was flanked by two perfusable channels and a mechanical actuator[32]. H. Lin et al. established an osteochondral unit on-a-chip. The study comprised two perfusion channels and two tissue compartments in a well-plate like platform. Bone and cartilage tissues were engineered from GelMa and hyaluronic acid laden with BM-hMSCs. Both tissues were stacked without a differential interface in between and dually perfused with bone and chondrogenic media. The bioreactor was secured in a well-plate-like system with two perfusion channels and the microtissues as removable inserts. Once the platform was established, pro-inflammatory cytokines were added to induce inflammation to mimic OA[33].

The field of organs-on-chip is rapidly advancing with the development of novel biofabrication technologies. Nevertheless, literature in osteochondral perfusable units is limited. The joint environment is complex, with many relevant tissues contributing to both health and disease of the joint and many metabolic processes still to decipher. There are still no reports of fluidic systems that recapitulate the interaction in an osteochondral unit with trabecular bone, osteochondral interface and hyaline cartilage. Several studies have described the role of the osteochondral interface in the development of disease in the knee joint, therefore it is hypothesized that the incorporation of the interface tissue in a perfusable osteochondral unit will better recapitulate the interplay in both health and disease. Thus, the establishment of a novel *in-vitro* model for the knee joint.

RESEARCH AIMS

We hypothesize that a bioprinted construct with two perfusable compartments, one bone and one cartilage with the presence of an osteochondral interface linking bone and cartilage will allow to recapitulate salient cell behaviours observed *in vivo* in healthy and pathologic joints, thus serving as a new drug testing platform.

To tackle such an ambitious aim, the project has two different phases, a) the engineering and optimization of the trabecular bone and osteochondral interface and b) the design, printing and assembly of the perfusion platform. Different fabrication methodologies will be used for the joint's components and bioreactor development such as hydrogel casting, volumetric bioprinting (VBP), digital light printing (DLP) and silicon moulding with PDMS. Three key challenges to the generation of a knee joint *in-vitro* model have been identified: Diversity of structures to replicate with different ECM compositions and cell types and the delivery

of appropriate nutrients and signalling molecules needed to maintain phenotype in each tissue. The establishment of a dually perfused *in-vitro* model will help address the current shortcomings in preclinical testing and enable better understanding of the crosstalk in the knee joint environment both in health and disease.

MATERIALS AND METHODS

1. Cell culture

1.1 Cell culture of human immortalized Mesenchymal Stem Cells (iMSC), bone marrow derived human mesenchymal stem cells (hBM-MSC) and articular cartilage progenitor cells (ACPC). Both iMSC and BM-hMSCs were cultured at 37ºC and 5% CO2 incubator with 3x week media change. Expansion media is comprised of alpha-MEM (or DMEM + pyruvate) (Gibco) supplemented with 10% Fetal Bovine Serum (FBS) (Gibco), 5% Penicillin/Streptavidin (Gibco), 5% ASAP (Sigma) and 1µ/mL basic Fibroblast Growth Factor (bFGF). Conditions are similar for ACPC cell culture, media will be changed 3x week and will contain: DMEM + pyruvate, 10%FBS, 1% Pen/Strep, 1% ASAP, 1% Non-essential amino acids (NEAA) and 5µ/mL bFGF.

1.2 Trypsinization: To detach cells from the culture flasks cells are first washed with warm PBS. Once washed, we add 2mL of trypsin-EDTA (Gibco) per T-175 flask and incubate 2/5 minutes (depending of cell type) at 37ºC. Then tap the flasks on the sides to promote cell detachment. Once cells are detached a "curtain" of fallen cells can be seen in the media. Resuspend each T-175 flask with 4mL of fresh media. To avoid collecting a slime MSC produce, the suspension is filtered using 100µm pore filters. Once collected, the suspension is centrifuged at 1500rpm for 4 minutes and the supernatant is discarded. Cells are resuspended in an arbitrary amount of expansion media and counted in an automatic cell counter.

1.3 Cryo-preservation (or cell freezing): Once cells are in suspension these will be centrifuged at 1500rpm for 4 minutes and the media discarded. Cells will then be resuspended in freezing media 40% cell culture media, 50% FBS and 10% Dimethyl Sulfoxide (DMSO). Cell densities will vary depending on the cell type and the number of cells to freeze, with a minimum of 1Mcells/vial. Each vial contains between 1 and 1.5mL. Vials need to be placed in a Mr. Frosty and placed at -80ºC overnight before being moved to liquid nitrogen, -180ºC, for long term preservation.

1.4 Cartilage differentiation from ACPC: To differentiate ACPC to chondrocytes they are first trypsinized and suspended in 5% GelMa at 15M cells/mL and 0,2% LAP. Then the gel suspension is casted in 3 Teflon moulds, 6 mm diameter and 2 mm height and photocured in a UV-oven for 15 minutes. The differentiation experiment has 3 time points, day0, day 14 and day 21. Media will be changed 3 times a week, the media will be composed of DMEM high glucose + pyruvate, 1%ITS Premix (Corning), 1% Pen/Strep (Gibco), 1% ASAP, 1% 1M HEPES (Gibco) and Dexamethasone, 1mg/mL in 100% EtOH (Sigma), add 1µL TGFβ1 per mL of media added fresh.

1.5 Selection of BM-hMSCs via bone differentiation: Three bone marrow samples were acquired from the University Medical Centre Utrecht (UMCU, The Netherlands) mean age 32.5 years old range 15-50. Anonymization was performed and tissues were obtained according with the ethics guidelines of the UMCU. Cells were isolated following an already described protocol[34]. The three donors were expanded and casted in hydrogel disks of 6mm diameter and 2 mm height, hydrogel 5% GelMA, 0.1% LAP with 5M cells /mL. Hydrogels were cultured in bone differentiation media with media changes 3 times a week. Differentiation media composition was: alpha-MEM (Gibco), 10% FBS, 1% ASAP, 1% Pen/Strep, 1% Glycerophosphate and 2µL dexamethasone added fresh.

2. Bioink preparation and optiprep

2.1 GelMa preparation: GelMA was synthesized according to the previously described protocol[35]. Prepared at desired concentration diluted in 0,1% LAP solution in PBS. When printing at high cellular densities, the refraction and light scattering of the suspended bodies results in lower print resolution, therefore Optiprep (Stemcell) is used. Optiprep modifies the optic properties of the solution, preventing a decrease in print resolution. Optiprep is added to the gel mixture at the desired concentration before printing, in this case 10, 20, 30 and 40% w/v.

2.2. Dual printing iMSC: Differentially dyed iMSCs were used for a preliminary study to print with two different cell types in two phases when using the VBP. To differentiate two different populations of iMSCs we used CellTracker CM-DiI and CM-DiD (ThermoFisher) according to manufacturer's protocol. Cell pellets were suspended in a PBS solution with 10% v/v of cellTracker and incubated for 20 minutes at 37ºC and 5% CO2. Labelled iMSCs were suspended in a solution of 5% GelMa and 0,1% LAP. CellTracker DiD was used to VBP 1Mcells/mL in a block gyroid 6x8mm with a light dose of 150 mJ/cm^2 and CellTracker DiI was used to print 2Mcells/mL in a disk at a light dose of 250 mJ/cm^2. Once the gyroid was printed, the DiI iMSCs labelled solution was added into the vial for a second round of printing for the disk. Prints were imaged using a Thunder microscope (Leica) at wavelengths of 640nm for DiD and 550-590 for DiI.

3. Paraffin embedding and histology

3.1. Dehydration and paraffin embedding: Store in Phosphate buffered formaldehyde 4% (Klinipath) for a minimum of 24 hours to a week maximum before dehydration. To dehydrate, 2 rounds, 30 minutes each of: 70% EtOH, 96% EtOH, 100% EtOH and leave in absolute ethanol overnight. Followed by two rounds of 30 minutes xylene (Klinipath) and 1.5 h paraffin (Stemcowax, Adamas Instrumenten) bath at 60ºC. Once incubated in paraffin embed in histology cassettes, cool down and cut with a microtome (Leica).

3.2. Von Kossa staining: For the observation of deposits of calcium or calcium salts. Deparaffination of histology slides two rounds of 5 minutes xylene, 2 rounds 3 minutes EtOH 100%, EtOH 96%, EtOH 70%, di-water and Rinse in tap water. Incubate slides with 1% silver nitrate (Sigma) in the UV oven for 20 minutes. Rinse the slides in several changes of distilled water before removing the unreacted silver nitrate with a 5 minute incubation in 5% Sodium thiosulphate (Sigma). Rinse in several changes of distilled water and counterstain with 50% solution of Meyer's haematoxylin (Merk) for 10 seconds. Then, rinse in running tap water for 10 minutes and several changes of distilled water. Dehydration by 2 rounds 3 minutes of EtOH 70%, EtOH 96% and EtOH 100% followed by two rounds of 5 minutes xylene. Once dehydrated use mounting media and cover with a cover slip.

3.3. Safranin O and Fast Green Staining: Deparaffination is done by two rounds of 5 minutes xylene, then 2 rounds 3 minutes each EtOH 100%, EtOH 96%, EtOH 70% and di-water. Slides are then soaked in Weigert's Haematoxylin (Klinipath) for 5 minutes, rinse in running tap water for 10 minutes followed by a wash in distilled water. Incubate in 0,4% Fast Green FCF solution (MP Biomedicals) for 4 minutes followed by a series of washing with 1% Acetic Acid (Sigma-Aldrich) until no stain runs through. Incubate in 0,125% Safranin-O (Sigma-Aldrich) for 5 minutes. Wash in running tap water for 10 minutes and dehydrate.

3.4. Alkaline Phosphatase assay (ALP): Transfer cultured samples to an Eppendorf tube with 250 µL MPER buffer and bring to -80ºC storage. At day of assay, do a few cycles of freeze, thaw between -80ºC and 37ºC. To lysate the samples use a piston stored in 70% Ethanol, prepare two tubes of PBS-Tween 20 0.1% and two PBSO. Crush the thawed samples with the piston then clean by submerging in the four tubes between each sample. Dilute the pNPP and Tris-Buffer tablets (Sigma) in 20mL PBSO and prepare the standard curve of ALP enzyme with 50 µL ALP enzyme 8 U/mL. Perform serial dilutions of the enzyme until a concentration of 0.031 U/mL. Transfer 25 µL of the standard curve and samples to a 96 well plate in duplicate. Add 50 µL of the pNPP solution and read at both 405 nm and 655nm.

4. Biochemical analysis

4.1. Papain digestion: Add 250 µL of papain solution to each sample and incubate overnight at 60ºC. Vortex samples and incubate one hour at 60ºC.

4.2. PicoGreen assay for dsDNA quantification: Use already papain digested samples at room temperature. Prepare a stock solution of λDNA at a concentration of 1µg/mL (5 µL λDNA in 495 µL TE buffer) and standard curve. Dilute samples in 1x TE buffer, dilution factor 20x. Transfer 100 µL of each diluted sample to a 96-well plate. Dilute the PicoGreen reagent (ThermoFisher) 200x in TE buffer and add 100 µL to each well. Then incubate the well plate for 5 minutes covered from light and measure fluorescence at 485 nm excitation and 520 nm emission.

4.3. DMMB for quantification of glycosaminoglycans (GAGs): Use already papain digested samples at room temperature. Prepare standard curve of Chondroitin sulphate 1 to 0.0156 µg CS/well. Dilute the samples in PBS-EDTA and transfer 100 µL of both samples and standard curve to 96 well plate. Finally add 200 µL DMMB staining solution (Sigma Aldrich) to each well and measure extinction at 525 and 595 nm.

5. Mechanical testing, imaging and transport

5.1. Dynamic Mechanical Analysis (DMA): Samples were tested for DMA (Zwick Z010; Zwick Roell Kennesaw, USA) with a 1kN load cell for uniaxial compression at a stress/strain ramp 20-30%. The compressive modulus (or Young's modulus) was obtained from the slope of the linear section of the stress/strain curves.

5.2. Transport assay with µCT: Optiprep was used as contrast agent. This protocol is inspired on the work of Bleys et al from TU Delft in the effect of microarchitecture in solute transport properties[36]. Hydrogel disks were VBP, 10x10x4 mm in size, light dose of 250 mJ/cm^2. Once printed, constructs were post-cured for 15 under UV light in a solution of 0.1% LAP. Samples were placed in the µCT (Quantum FX; PerkinElmer, Waltham, MA, USA) with an optiprep droplet on top and imaged 0, 5, 10, 20, 30, 45 and 60 minutes, 26 second scans, voltage 90 kV, current 180 mA, FOV = 15. In the images, GelMa appears dark while optiprep appears white. For data analysis, the change in grey scale was measured in every image and plotted as light intensity vs hydrogel thickness in pixels (Fiji, Image J 2.0.).

5.4. FITC-Inulin transwell transport assay: Custom transwell inserts for a 48 well-plate were designed and printed with PLA using a Fused deposition modelling (FDM) 3D at 80% infill to avoid material absorbance by the PLA. Once printed, 40 µm pore membranes were inserted at the bottom of each transwell insert before gel casting. 10 and 15% GelMa with 0,1% LAP crosslinked under a point blue lamp for 5 minutes at an intensity of 80% with a height of 3mm. A stock solution of 1 mg/mL FITC-inulin was diluted in PBS to 25 µg/mL as a working solution. Once the gels were casted, 700 µL PBS was added to the basolateral compartment of the transwell (bottom of the well) while 300 µL 25µg/mL FITC-Inulin was added to the top of the gel. Negative control was a transwell insert with 40 µm pore membrane but no hydrogel. Transwells were incubated for 1 hour at 37 degrees while protected from any light source. Standard curve was prepared in serial dilutions of FITC-Inulin 25 µg/mL to 0,025 µg/mL. After an hour of incubation, samples were taken from the basolateral compartment and the standard curve, 100 µL in duplicate and transferred to a 96 well-plate. The well plate was read at excitation 485 nm and emission 538 nm.

6. Assembly of the perfusion platform

There are four hydrogel components to add to the perfusion platform. A DLP 3D printer (Prefactory, EnvisionTec) is used to print a negative mould of the hydrogel components' holder which will be filled with Polydimethylsiloxane (PDMS, Dow chemical company) to create the holder. PDMS elastomer and cross-linker are mixed at 9:1 ratio, stirred, degassed, poured in the mould and crosslinked at 60ºC for 3 hours or until solid.

The outer holder of the perfusion platform is 3D printed using an FDM Ultimaker S3, with polylactic acid (PLA). Printing parameters were 80% infill and print accuracy of 0.15, trihexagonal infill pattern. The bottom holder of the perfusion platform accounted with an indenture for a 60x70 mm glass slide and four 5Mx30mm screws. Both inner and outer holders have channels of 2mm diameter where to insert tubing of 2mm outer diameter and 1.5mm inner diameter.

The hydrogel components of the PDMS holder are crosslinked in the PDMS holder using a point blue lamp at 80% UV light intensity for 5 minutes. To avoid the liquid hydrogel from invading nearby compartments, PDMS stoppers are used. A block gyroid 8x6 is printed using a Volumetric Bioprinter and added to the PDMS mould once all other components are crosslinked.

All CAD designs were generated using Fusion 360 (Autodesk) and TinkerCAD (Autodesk).

Microbeads for perfusion are 125-150 nm in diameter and 450-500 nm in diameter (ThermoFisher) are prepared in a 0.1% Tween 20 (Sigma) solution in distilled water and stored at room temperature.

RESULTS AND DISCUSSION

1. Optimization of the volumetric bioprinting (VBP) conditions for iMSC and BM-hMSC, differentiation of volumetrically printed BM-hMSC.

The present section involves the optimization of VBP for BM-hMSC laden 5% GelMA. Several steps were needed to optimize the printing process. The presence of cells or opaque bodies increases the light scattering in the hydrogel and affect the resolution of VBP. The printing resolution decreases as the light-scattering in the bioink increases. Iodixanol is an optic property modifier used to mitigate the effect of turbidity without damaging cells[37]. The first optimization of iodixanol concentration is in iMSCs (Figure 1), iMSCs have similar properties to BM-hMSCs, grow to larger numbers and are overall more resilient to manipulation than hMSCs[38]. Therefore, iMSCs are commonly used to obtain preliminary data to later experiment with hMSCs. In this case, iMSCs were used to optimize iodixanol concentration and limit the study groups used for BM-hMSCs (Figure 2). Once the optimal iodixanol concentration to VBP hBM-MSC was established, several architectures are printed and differentiated towards osteogenic lineages (Figure 3).

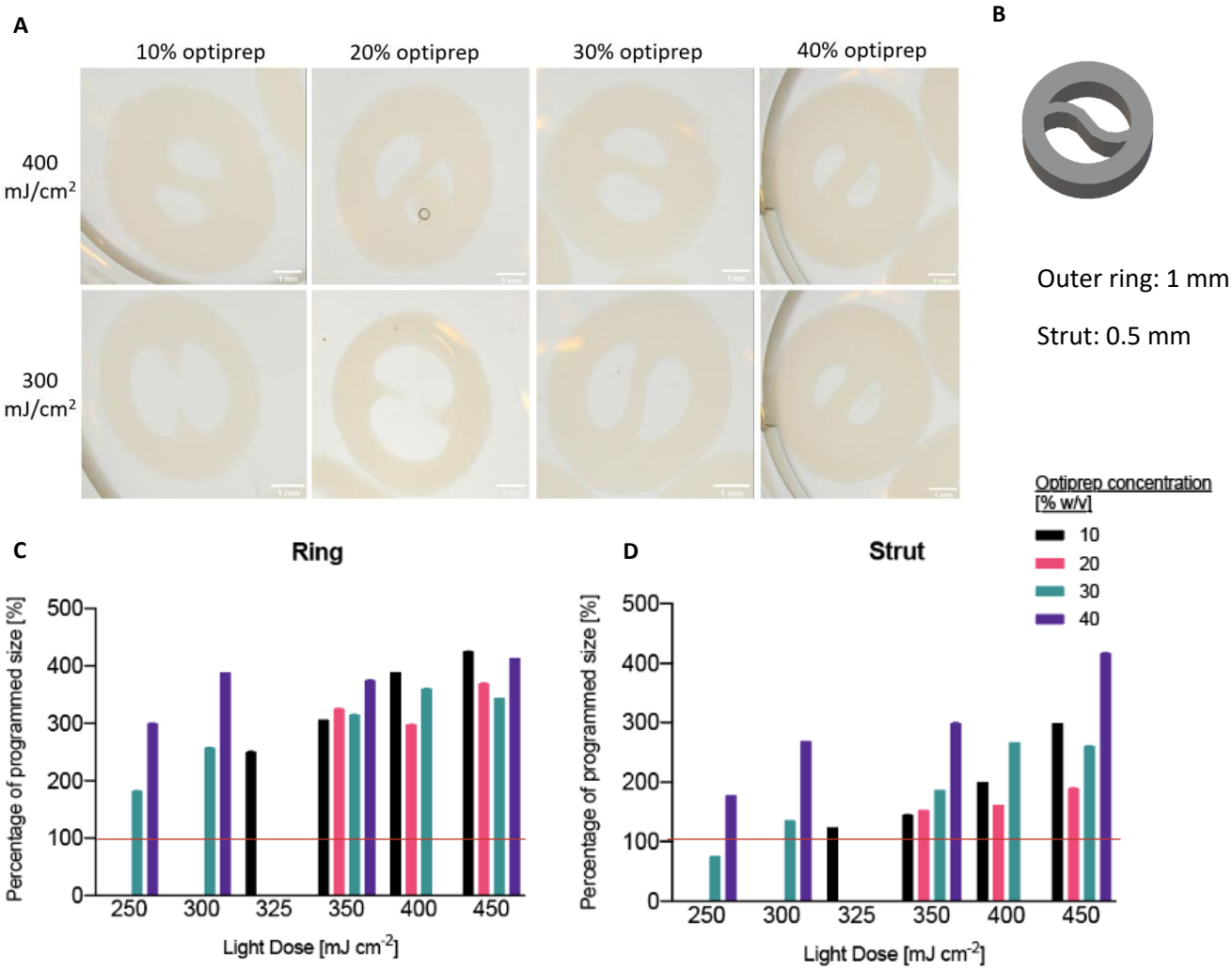

Figure 1: VBP of 5M hiMSCs/mL with 10, 20, 30 or 40% w/v of iodixanol in 5% GelMa hydrogels. A) Pictures of the obtained hydrogels with 10, 20, 30, or 40% iodixanol w/v at two different light exposures 300 and 400 mJ/cm^2. Scale bar 1mm. B)

Original design for the prints with measures, 1 mm for outer ring thickness and 0.5 mm for strut thickness. C) Overpolymerization coefficients of the prints, measures taken from the outer ring and compared to the STL file, in percentage. Red line marks the original design's measures. D) Overpolymerization coefficients of the prints, measures taken from the strut and compared to the STL file, in percentage. Red line marks the original design's measures.

Figure 1 A show how prints obtained at higher light doses are thicker than those obtained at lower light doses. Longer exposition times create bigger prints, while shorter expositions lead to incomplete features. Examples of under-polymerization are in Figure 1 A, 300 mJ/cm2 neither 10 or 20% w/v iodixanol achieve crosslinking of the strut. When the light dose increases by 100 mJ/cm2 (to 400 mJ/cm2), all iodixanol conditions fully represent the original design. Figures C and D give an overview of the overpolymerization and its relation to iodixanol concentration and light dose. Both graphic representations in C and D show how much bigger the prints are compared to the original design in percentage. 30% iodixanol is the concentration that achieves better print fidelity across the four tested concentrations. Furthermore, both 30 and 40% iodixanol achieve prints at lower light doses than other concentrations. Iodixanol is not toxic to cell cultures[37]. The use of low-level laser irradiation has also been shown not to be toxic to MSCs[39]. None of the parameters considered in this section has a significant negative effect on the viability of cellular constructs, thus the choice of iodixanol concentration is determined by the size comparison in Figure 1 C and D. The concentration of iodixanol with better shape and size fidelity is 30%. At 30% iodixanol, the prints are resolved at lower light exposures, with the lowest size variability across all iodixanol groups. Thus it is considered to be the most appropriate condition. At the lowest light dose of 250 mJ/cm2, the outer ring is resolved at 170% while the strut is resolved at 80%. 20% iodixanol resolves structures with good shape fidelity but the resolution at 325 mJ/cm2, is lower, thus the overpolymerization is higher than with other iodixanol concentrations. 40% iodixanol shows an increase in feature size at low light expositions compared to the other conditions. This composition could print at even lower light exposures and result in features resolved at a similar size than 30% or closer to the original design. A limiting factor in this study is the availability of cells to incorporate in the bioink. Therefore, further printing with the same bioink condition was not possible. It is hypothesized that a concentration of 40% w/v of iodixanol in the bioink has the potential for printing at lower light doses than 30% and resolve features with matched or increased size similarity than 30%.

In light of the results obtained in figure 1, the optimal concentration of iodixanol to VBP a bioink composed of 5% GelMa, 5 million iMSC/mL and iodixanol is 30%. Nevertheless, it is possible that 40% iodixanol has the capacity of resolving features with similarly fine features than 30%. Further experiments with BM-hMSC will use both 30 and 40% w/v iodixanol as part of the bioink composition.

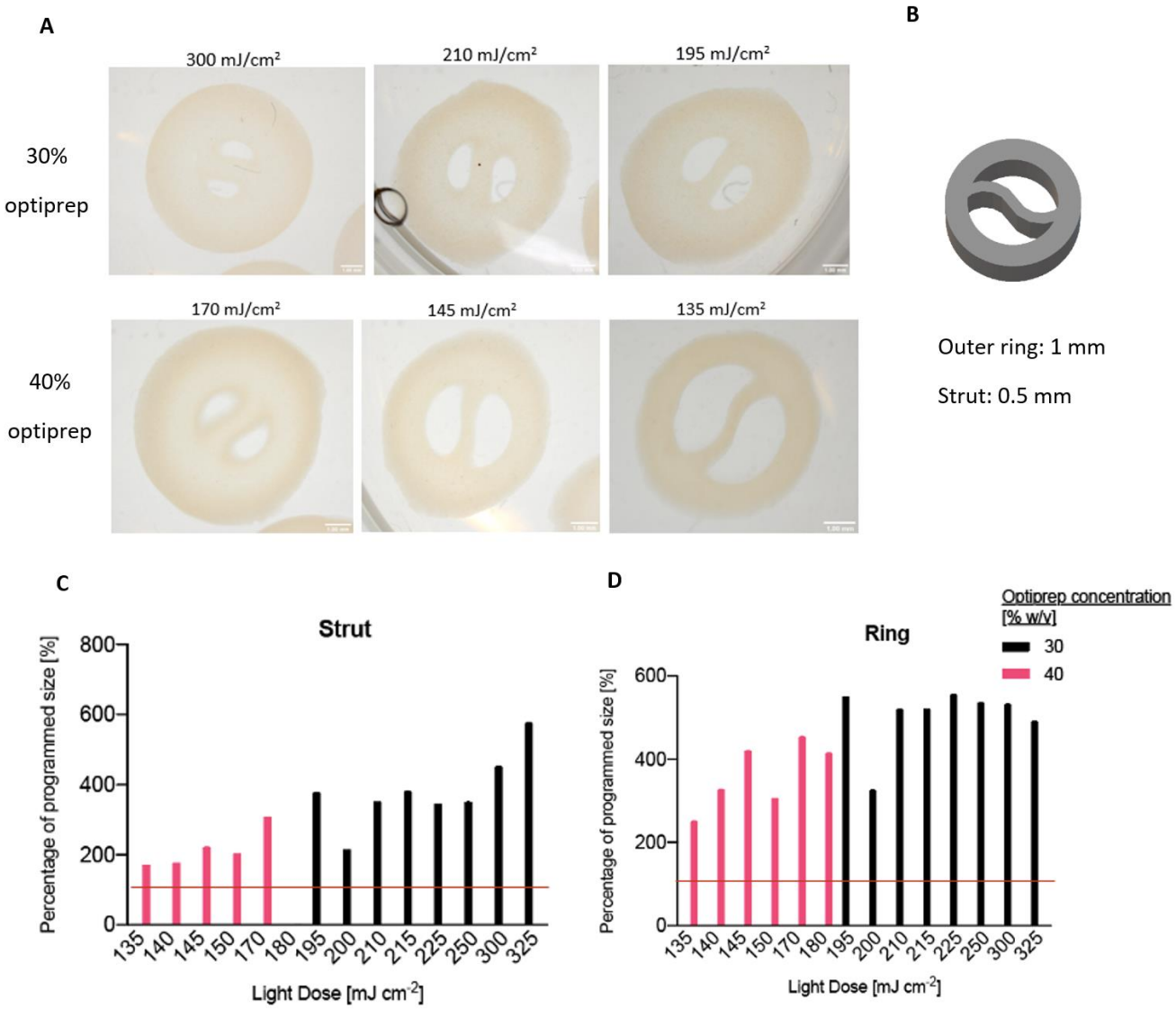

Figure 2: VBP of 5M BM-hMSCs/mL in 5% GelMA with 30 and 40% w/v iodixanol. A) Different combinations of optiprep concentration and light dose in mJ/cm^2. Scale bar 1mm. B) Original design for the prints with measures. C) Overpolymerization coefficients of the prints. Red line indicates 100% programmed size, which corresponds to the size of the original design. C) Overpolymerization coefficients of the prints, measures taken from the strut and compared to the original design, in percentage. Red line indicates 100% programmed size, corresponding to the size of the original design.

Figure 2 shows the VBP of 5 million BM-hMSC/mL in two concentrations of iodixanol, 30 and 40%. Figure 2 C and D show the overpolymerization rate of the prints at different light exposures. Contrary to as seen in Figure 1, both iodixanol concentrations do not overlap in light exposure. The bioink with 40% iodixanol prints at much lower light doses than 30% w/v iodixanol, 135 mJ/cm2 against 195 mJ/cm2. As seen in Figure 1, the limiting factor when optimizing the VBP of cell-laden bioinks is the availability of cells. Here, 30% iodixanol could have been printed at lower light doses. Nevertheless, low availability of bioink did not allow for testing of lower doses. The bioink composition with 40%w/v iodixanol achieves prints that closely resemble the programmed size of the original design. At 135 mJ/cm2, the overpolymerization of the strut was 150%, while the overpolymerization of the outer ring was 230%. There is a significant difference between the overpolymerization coefficient of the strut and the outer ring. Such phenomenon can be explained by the accumulation of light dose where the features of the design meet, where the strut meets the ring. The accumulation of light to resolve both features yields local overpolymerization resulting in the protuberances

seen in the images in Figure 2 A, that give the ring a slightly elongated shape reminiscent of lemons. From the observations in Figure 2, the optimal concentration of iodixanol to VBP 5 million BM-hMSCs is 40% w/v due to shape and size fidelity to the original design. Therefore, all experiments using BM-hMSC in a 5% GelMa bioink for volumetric bioprinting will use 40% w/v iodixanol in the bioink composition. Once the composition of the bioink for 5 million BM-hMSC was established, three different designs were printed in the VBP and differentiated to bone for 21 days.

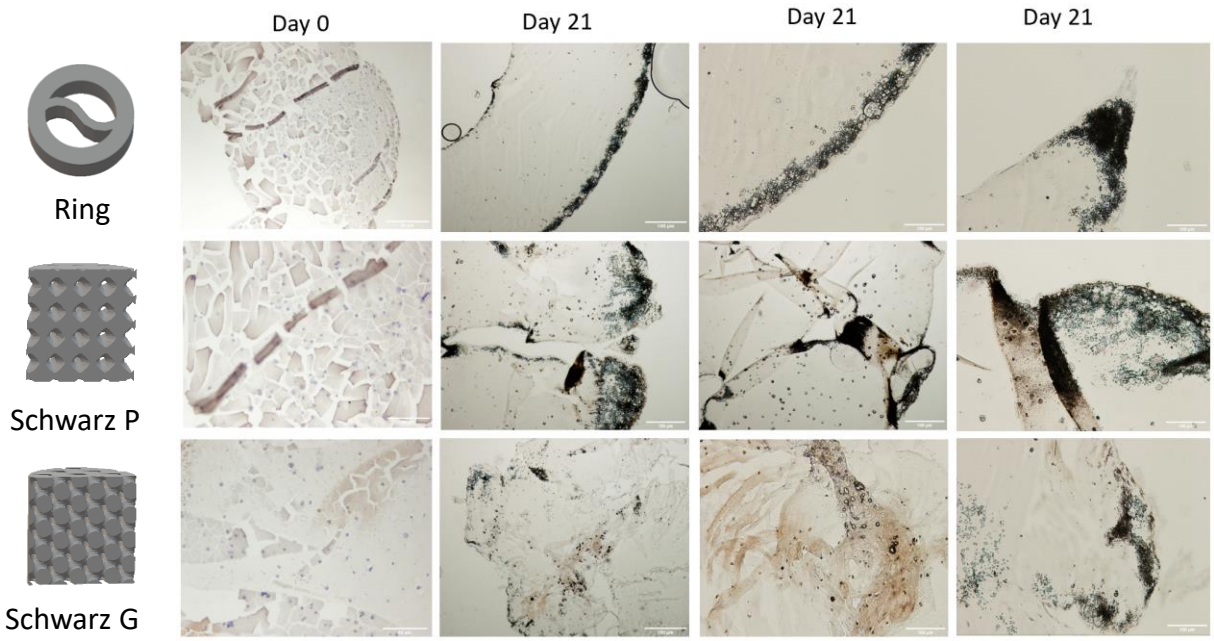

Figure 3: Bone differentiation of VBP 5M BM-MSCs/mL in a 5% GelMa, 40% w/v iodixanol bioink at a light dose of 155 mJ/cm^2. Printed designs and Von Kossa staining of bone differentiation of the prints at day 0 and day21. Scale bars represent 50 µm in day 0 pictures and 100 µm for day 21.

Figure 3 has the images obtained from the Von Kossa staining of VBP differentiated to bone for 21 days. Staining from samples on day 0 of culture serve as negative differentiation controls. The Von Kossa histology staining show calcium deposition in black while semi-calcified cytoplasm and cell nuclei appear in brown/red[40]. The images in figure 3, show that the differentiation in the samples is scarce. The majority of the staining signal is at the borders of the prints rather than being homogeneously distributed. The culture of the prints in differentiation media was in standard static conditions. Therefore, it is possible that bigger prints, as the gyroids, could impair fluid transmission due to print thickness or pore occlusion. It could also be that the differentiation media could have not been optimal for bone differentiation of BM-hMSC. Nevertheless, the same media composition was successfully used in Supplementary figure 1 to differentiate three different donors of BM-hMSC to bone. Therefore, the media composition could not have contributed to the lack of bone differentiation in the VBP. Several studies have focused on the effects of volumetric bioprinting in cells and shown high viability after printing, post-curing and short term culture[41]. Other studies have focused on the differentiation of MSCs towards osteogenic lineages with successful results[42]. The printing process has proven to be safe and effective at producing highly viable and active scaffolds, while the used differentiation media has been tested successfully in other instances. Nevertheless, the present study fails to reproduce bone differentiation in the printed constructs. Might be that the cells received damage during the trypsinization or post-curing process that has been unaccounted for in other studies.

The last study involving Volumetric Bioprinting was a preliminary attempt to optimize the printing of two different bioinks sequentially to obtain one single structure with different characteristics, material compositions. For the study two differently labelled populations of iMSCs in 5% GelMa were used.

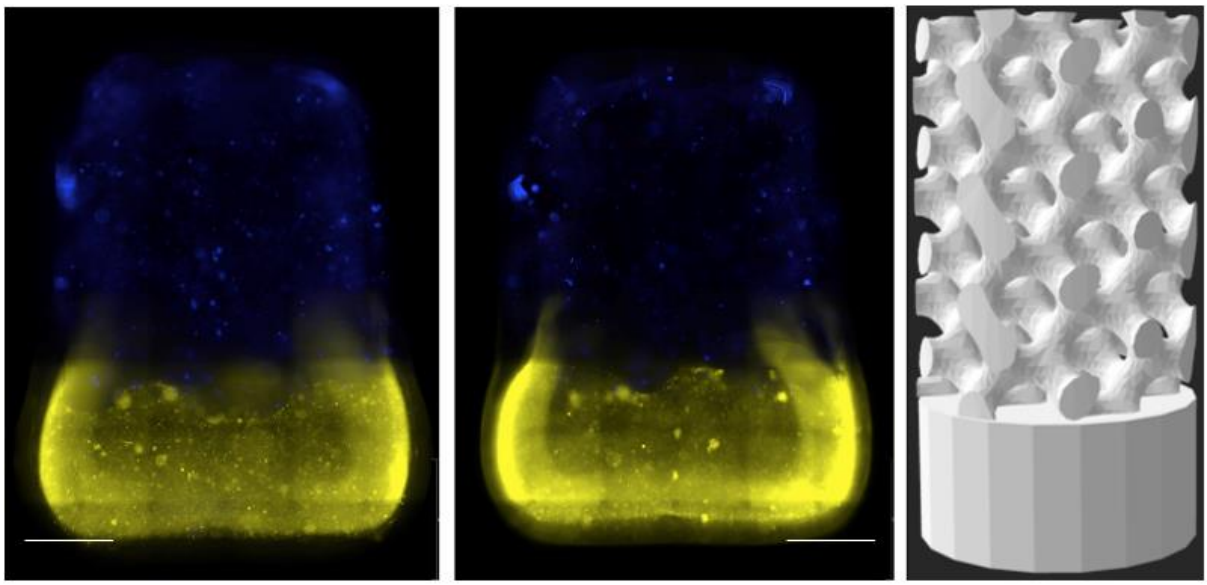

Figure 4: Dual printing VBP of differentially labelled iMSC in 5% GelMa. In yellow, 2M cells /mL labelled with CellTracker DiI, in blue 1M cells/mL labelled with CellTracker DiD. Scale bars 1mm. a) Dual VBP, combination of gyroid block 6x8 and a cylinder 6x6x3 mm. b) Dual VBP combination of gyroid block 6x8 and a cylinder 6x6x3 mm. Images taken with Thunder microscope (Leica).

Figure 4 is proof that the sequential addition of two bioinks is possible in volumetric bioprinting. It allows for the generation of structurally sound constructs. The images in figure 5 show a small overlapping area between designs corresponding to two differentiated regions with two different cell populations. The overlap between both layers appears to be the minimum necessary to guarantee print attachment and maintain the designs together as one print. This preliminary study shows how it is possible to use VBP to generate constructs with two different materials and potentially different cell types. A dual VBP approach can be beneficial to develop new avenues in reconstructing complex microarchitectures found in the physiologic state. Dual printing can be used for scaffold vascularization, spatially controlled delivery of cells and ECM components or patterning of differentially layered tissues[43] [44] [45]. The further development of dual volumetric bioprinting can impact a myriad of areas in tissue engineering. This project aims to dually VBP trabecular bone and osteochondral interface in one construct. The printing of these two structures in one same construct would enhance attachment, reduce leakage between bone and interface and potentially favour tissue maturation by the influence of the cells populating the bone compartment.

2. Material optimization for the osteochondral interface.

This section focuses on the optimization of candidate materials for the osteochondral interface. According to literature, the native osteochondral interface has a diffusion limit between 500 and 2000 Da[46]. Here, iodixanol and FITC-Inulin have been used to test whether the candidate materials were permissive to the passage of molecules under 2kDa in molecular weight.

Figures 5 A to D correspond to the transport of iodixanol through disks of both 5 and 10% GelMa at different times of incubation. In images A and B, it is seen how iodixanol visually penetrates through the hydrogel as incubation time advances. Figures 5 C and D are quantification of the light intensity produced by the iodixanol as it advances through the height of the gel. The aim of figures A-C and B-D is to decipher if both GelMa compositions are differentially permeable to iodixanol. From the quantification in the graphics, it is seen how both compositions are permeable to iodixanol and allow its gradual passage.

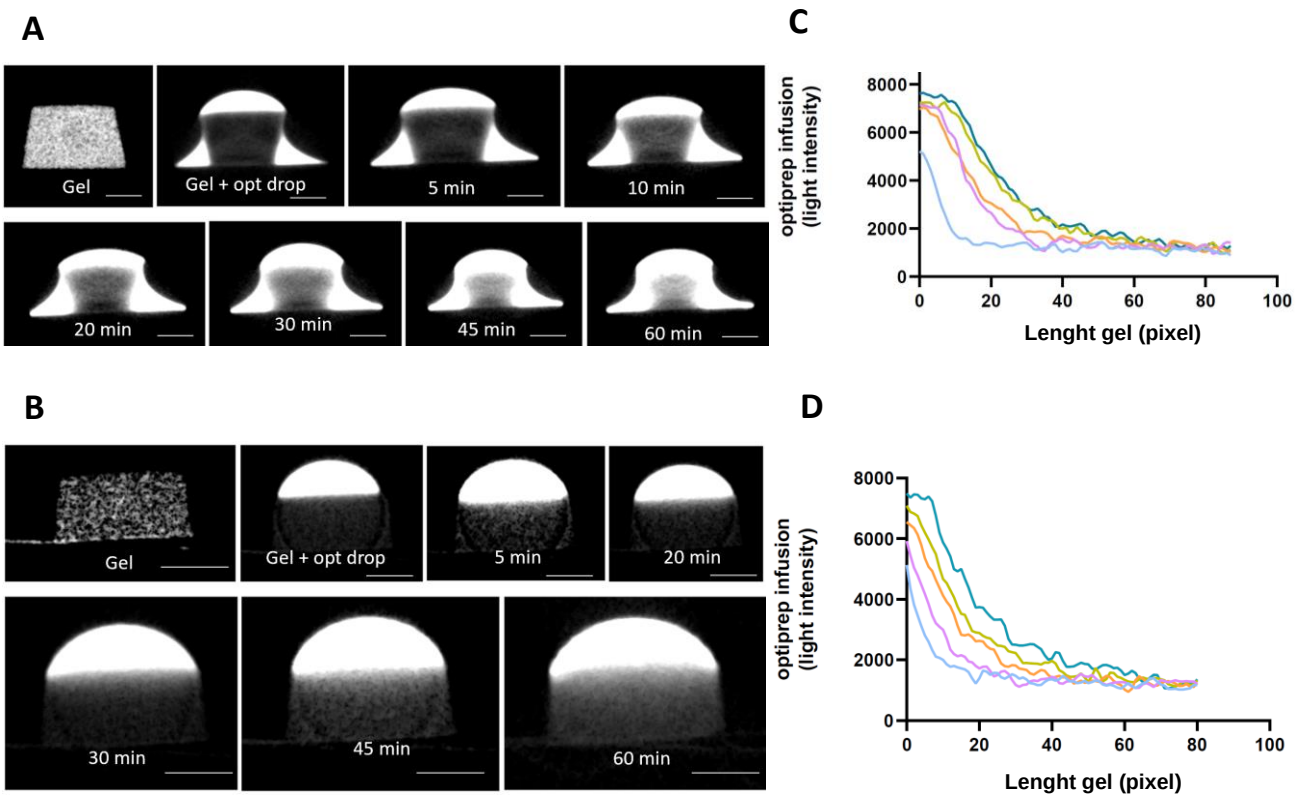

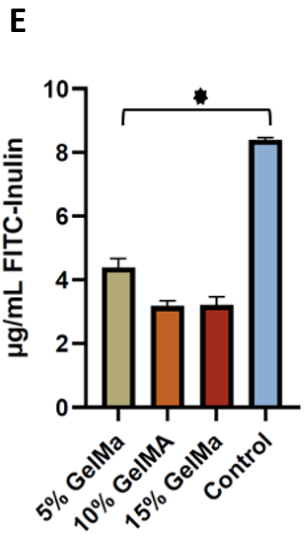

Figure 5: Transport study in 5 and 10% GelMa. A) 5% GelMa disks, in grey, imaged in µCT for their permeability to 60% iodixanol, in white. Scale bar 3mm. B) 10% GelMa disks, in grey, imaged in µCT for their permeability to 60% iodixanol, in white. Scale bar 3mm. C) Grey scale analysis across the height of the hydrogel light intensity plotted using Fiji – Image J at different incubation times. D) 10% GelMa incubated with 60% iodixanol. Light intensity plotted against hydrogel height in pixels. Measurements taken at different incubation times. E) FITC-Inulin transwell assay at 5, 10 and 15% GelMa. P-value < 0.05 between control and gel samples.

It is also seen how longer times of incubation, for example, 5 minutes vs 45 minutes have an impact on the length of hydrogel that the iodixanol is able to reach suggesting that the transport would eventually infuse the entirety of the hydrogel. Figure 5 E corresponds to the transport of FITC-Inulin in 5, 10 and 15% GelMa. From the graphic, it is seen how the hydrogel samples do allow transport of FITC-Inulin to a certain extent. There is statistical significance when the transport of FITC-Inulin is compared to the transport quantified in the negative control. Therefore, the presence of hydrogel does hamper the transport of FITC-Inulin in an hour incubation time. Nevertheless, there is no statistical significance in the difference in FITC-Inulin transport between gel conditions. All gel conditions are similarly permeable to 2-5 kDa molecules. FITC-Inulin has a range of molecular weights, from 2 to 5 kDa, therefore it is possible that the hydrogels are permissive to the lower end of the molecule spectrum. On the other hand, it is also possible that the hydrogel only slows down the passage of molecules which in time would eventually all diffuse through the gel. The aim of the study was to find a material that would transport 1500 Da molecules (iodixanol) but not be permissive to the diffusion of molecules bigger than 2kDa (FITC-Inulin). The aim of the study has been partially achieved with materials that gradually diffuse iodixanol and are partially permissive to FITC-Inulin. In light of the results, 10% GelMa will be used as osteochondral interface material. 10% GelMa shows to perfuse iodixanol at a slightly slower rate than 5% and have lower values of FITC-Inulin transport

(with no statistical significance). To improve the transport properties of the materials, a reinforcing agent could be added to the hydrogel as furfurylamide grafted chondroitin sulphate or maleimido-terminated poly(ethylene glycol)[47]. These materials form through supramolecular interactions and have been documented to increase the mechanical properties of materials without altering their water content. Such materials could be used to reinforce the structure to have a narrower exclusion to diffusing molecules.

3. Design and assembly of a dually perfusable bioreactor platform.

The last step in the project was to design and assemble a dually perfusable bioreactor platform. The platform integrates four compartments known to be affected by KOA. As described in the introduction, the compartments to mimic in the chamber are trabecular bone, osteochondral interface, and hyaline cartilage. The development of this project has focused on the trabecular bone and osteochondral interface. While unsuccessful attempts at cartilage differentiation have been made (supplementary figure 1), improvements need to be done in that avenue. The custom-designed bioreactor has four compartments, as seen in figure 6 C, D is the trabecular bone compartment, a VBP gyroid structure, A is the osteochondral interface, 10% GelMA, B is the cartilage layer, and C is the synovial space which is substituted by 5% GelMa. The platform has two perfusable channels that will provide media to all structures, through A there was flow to the bone compartment and through B-C to the cartilage. The platform was aimed to be leak-free to the outside, in between the bone compartment and the osteochondral interface. To achieve such an aim, the components seen in Figures 6 A and B were designed. Fig 6 B is the inner PDMS holder where the hydrogel components are added (seen in Figure 6 C) and a PDMS lid to ensure no contact of the exterior with the hydrogel components. To support the inner PDMS holder and create a sealed bioreactor, the holder in Figure 6 A is custom designed and 3D printed to tightly fit the inner holder. For further clarity on the platform's assembly, schematics are provided in figure 6 D. There, the construction of the platform in layers is seen. The inner PDMS holder with the hydrogel components (Figure 6 B and C) is inserted in the PLA holder (Figure 6 A) with a glass slide sealing the interface between PDMS and PLA. Four screws close the platform and the tubing can be inserted.

To decipher whether the platform was leak-tight or not, two different sized fluorescent microbeads were perfused through the channels. The aim of the microbead perfusion was to see if small microbeads from the bone compartment would cross to the cartilage compartment through the osteochondral interface (Figure 6 E). The platform proved to be leak-proof in all interfaces during short term perfusion. During assembly of the platform, any mode of insertion of the osteochondral interface as an insertable sheet resulted in leakage of microbeads to the cartilage compartment. Therefore, the approach to 3D bioprint the gyroid for trabecular bone and the osteochondral interface as a single dual VBP (Figure 4) changed. The osteochondral interface material was directly crosslinked in the PDMS inner layer (Figure 6 C). This new method of inserting the osteochondral interface in the system resulted in no microbead leakage between both compartments. Figure 6 E shows how the gyroid in the bone compartment is perfused with small microbeads which cover the whole structure and do not traverse to the cartilage compartment. The second compartment, perfused with bigger microbeads is proof that the platform can be independently perfused from the first one and was also leak-proof. No leakage was found around the platform or between components during short term perfusion.

The assembly and perfusion of the platform with fluorescent microbeads is a preliminary test to establish a bioreactor setup for the long term perfusion of cellular constructs for the four mentioned tissue types. The study shown in figure 6 E has proven that the proposed design is leak-proof and allows for dual perfusion of the two independent chambers. The future perfusion of cellular structures in this proposed platform will have to account for ease of fabrication or assembly to maintain leak tightness. The osteochondral interface needs to seal both perfusable compartments and only allow passage of 2kDa molecules. The solution found during development was to crosslink the candidate hydrogel directly in the platform, therefore eliminating the risk of fluid accumulation in corners or vertices. The same approach was adopted for the other two

hydrogel compartments the cartilage hydrogel was also directly crosslinked. Future versions of the platform will involve the addition of cellular constructs for the cartilage and synovium. The cellular constructs will be statically cultured and inserted for perfusion testing or seeded and cultured directly in the perfusion platform. Both approaches have challenges, the culture of the scaffolds and later insertion in the platform has the risk of compromising the platform's leakage. While the culture of the scaffolds in the platform has the challenge of long term (up to 28 days for cartilage differentiation) sterile culture in a leak-free system.

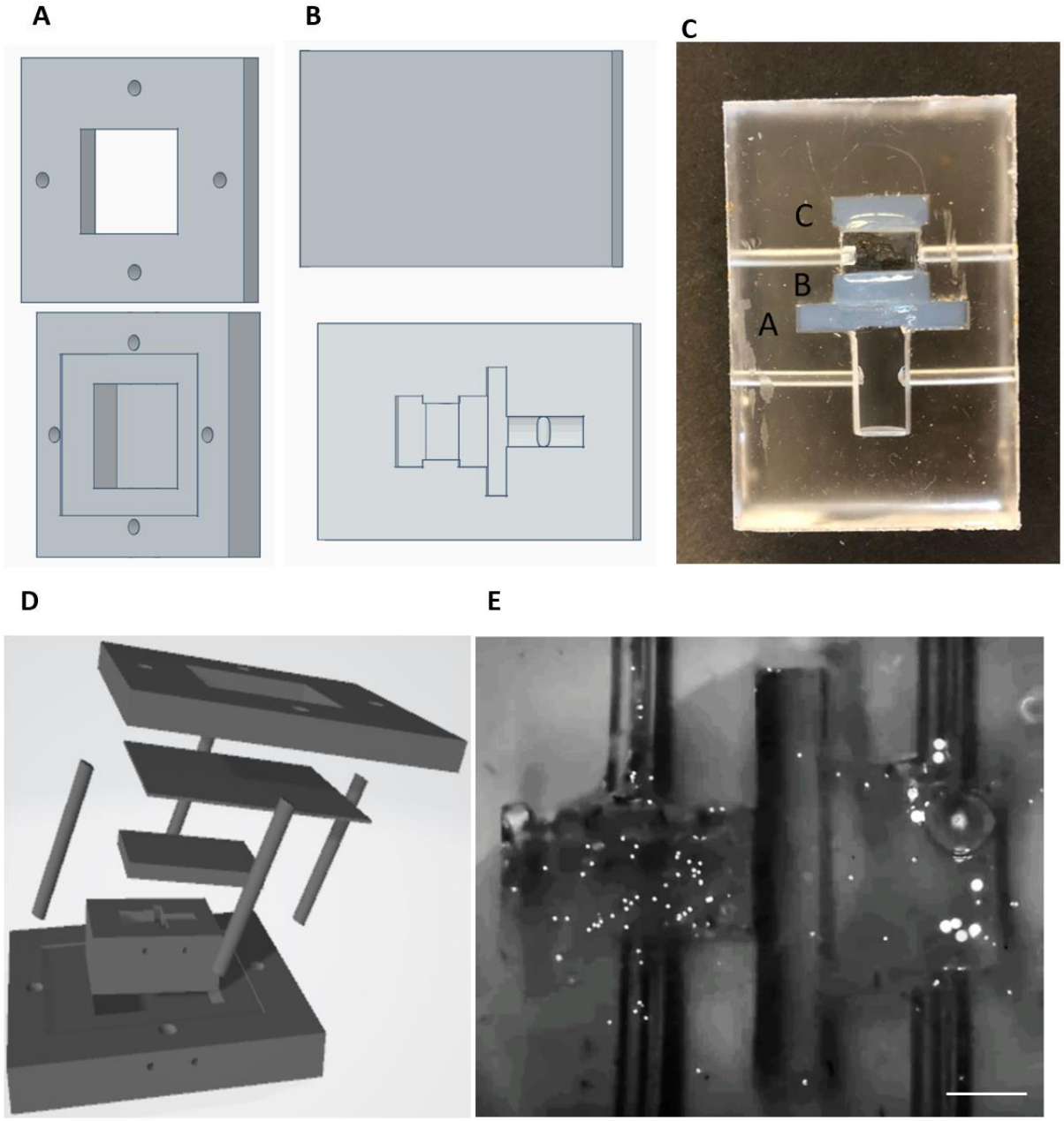

Figure 6: Assembly of the custom perfusable platform. A) Outer holder of the perfusion system. B) Inner PDMS holder for the hydrogel components. C) Inner PDMS mould seen in Figure 7 B with three of the components crosslinked in the platform, scale bar represents 5 mm. D) Schematic of the assembly of the perfusion platform. Bottom PLA holder with PDMS inner holder and dented lid, 60 x 70 mm glass slide, top PLA holder and 4 x 5M screws 30mm length, 2mm outer diameter tubbing for perfusion. E) Capture of perfusion video, bone compartment contains a block gyroid where fluorescent microbeads 125-150 µm diameter are perfused at 6 µL/min flow rate. Cartilage compartment perfused with 400-450 µm diameter beads with a syringe by hand. Scale bar represents 5 mm.

GENERAL CONCLUSIONS AND FUTURE DIRECTIONS

The research aims established at the beginning of the project have been achieved. Volumetric bioprinting has been optimized for BM-hMSC-laden hydrogels and, different compositions have been assayed as candidate materials to engineer the osteochondral interface. On the other hand, a dually perfusable bioreactor platform was designed and assembled, resulting in a leak-free system both at the interfaces of the platform's components and between the two perfusable compartments.

The differentiation of a cartilage construct (supplementary figure 1) and the differentiation of BM-hMSCs volumetric prints to bone (Figure 3) were not successful. Thus, new attempts at differentiating both compartments are needed. Similarly, the perfusion platform has only perfused in the short term. While the platform has proven leakproof in short perfusion terms, this is no guarantee that the platform will not leak when undergoing longer perfusion (up to or more than 24 hours). The leak tightness of the platform is a limiting factor to the establishment of a reliable in-vitro model. To sustain perfusion of a differentiated tissue construct and obtain valuable information on the maintenance of a health state or development of disease, it is of paramount importance to achieve long term perfusion. Another challenge to the assembly of the perfusion platform is to incorporate the cellular scaffolds. Two challenges are identified, the assembly of already differentiated scaffolds and the differentiation of those scaffolds in long term perfusion.

The completion of this project sheds light on the development of a novel in-vitro model to study the interplay between the tissues found in the knee joint environment that are most commonly affected by KOA. The further development of the proposed platform with the incorporation of cellular scaffolds in long term culture will represent a one-of-a-kind novel in-vitro model. Four different tissues will be engineered and perfused with two media. Contrary to the model proposed by H. Lim et al[33]. This model includes a scaffold for the osteochondral interface and a synovial space, missing in the model by H. Lim et al and could provide further information about the homeostasis on the joint. Furthermore, the proposed platform could serve as a model to develop other in-vitro models with up to four sequential tissues. MINI-JOINT provides an avenue to develop novel in-vitro models that recapitulate the complexity of tissue systems.

AKNOWLEDGEMENTS

The completion of this project has been challenging. The internship has been long and deeply affected by the COVID-19 pandemic and the struggle of having a part-time job during such a demanding and interesting experience. Nevertheless, the successful completion of the project which culminates in the delivery of the manuscript would have not been possible without an incredible support system.

First of all I would like to thank my supervisor Paulina Nuñez Bernal and my first examiner Riccardo Levato for accepting me in the project and encouraging development as a future scientist. I would also like to thank my co-workers in the lab, both pHD students and interns, Anneloes Mensiga for technical support, Gabriel Grossacher for thoroughly helping in some 3D printing applications and design, also for innumerable coffee and drinks outside of the laboratory. I would also like to thank Ona and Dieuwke, Manu, Elianne and Bea for sharing the struggle of being an intern. And Marc, Davide, Margo and Gerardo for guidance in some experiments.

Last but not least I would like to thank my family for supporting my career outside of my country and financing my education. Also to Lars De Boom, Irish Joy, Judith Calvo and Gloria Carta for their priceless support, love and appreciation through many ups and downs.

REFERENCES

1. Volksgezondheidenzorg. Prevalence of KOA in huisartsenpraktijk. (2019).
2. Bijlsma, J. W. J. & Knahr, K. Strategies for the prevention and management of osteoarthritis of the hip and knee. *Best Practice and Research: Clinical Rheumatology* (2007) doi:10.1016/j.berh.2006.08.013.
3. Magnusson, K., Turkiewicz, A. & Englund, M. Nature vs nurture in knee osteoarthritis – the importance of age, sex and body mass index. *Osteoarthr. Cartil.* (2019) doi:10.1016/j.joca.2018.12.018.
4. Mora, J. C., Przkora, R. & Cruz-Almeida, Y. Knee osteoarthritis: Pathophysiology and current treatment modalities. *Journal of Pain Research* (2018) doi:10.2147/JPR.S154002.
5. Goodman, S. M. *et al.* 2017 American College of Rheumatology/American Association of Hip and Knee Surgeons Guideline for the Perioperative Management of Antirheumatic Medication in Patients With Rheumatic Diseases Undergoing Elective Total Hip or Total Knee Arthroplasty. *Arthritis Rheumatol.* (2017) doi:10.1002/art.40149.
6. Piluso, S. *et al.* Mimicking the Articular Joint with In Vitro Models. *Trends in Biotechnology* (2019) doi:10.1016/j.tibtech.2019.03.003.
7. Dulay, G. S., Cooper, C. & Dennison, E. M. Knee pain, knee injury, knee osteoarthritis & work. *Best Practice and Research: Clinical Rheumatology* (2015) doi:10.1016/j.berh.2015.05.005.
8. Findlay, D. M. & Kuliwaba, J. S. Bone-cartilage crosstalk: A conversation for understanding osteoarthritis. *Bone Research* (2016) doi:10.1038/boneres.2016.28.
9. Steinmetz, K. L. & Spack, E. G. The basics of preclinical drug development for neurodegenerative disease indications. *BMC Neurol.* (2009) doi:10.1186/1471-2377-9-S1-S2.
10. Wilmer, M. J. *et al.* Kidney-on-a-Chip Technology for Drug-Induced Nephrotoxicity Screening. *Trends in Biotechnology* (2016) doi:10.1016/j.tibtech.2015.11.001.
11. King, S. M. *et al.* 3D proximal tubule tissues recapitulate key aspects of renal physiology to enable nephrotoxicity testing. *Front. Physiol.* (2017) doi:10.3389/fphys.2017.00123.
12. Moroni, L. *et al.* Biofabrication strategies for 3D in vitro models and regenerative medicine. *Nature Reviews Materials* (2018) doi:10.1038/s41578-018-0006-y.
13. Braun, H. J., Kim, H. J., Chu, C. R. & Dragoo, J. L. The effect of platelet-rich plasma formulations and blood products on human synoviocytes: Implications for intra-articular injury and therapy. *Am. J. Sports Med.* (2014) doi:10.1177/0363546514525593.
14. Kohli, N. *et al.* Bone remodelling in vitro: Where are we headed?: -A review on the current understanding of physiological bone remodelling and inflammation and the strategies for testing biomaterials in vitro. *Bone* (2018) doi:10.1016/j.bone.2018.01.015.
15. Maletsky, L. *et al.* In Vitro Experimental Testing of the Human Knee: A Concise Review. *The journal of knee surgery* (2016) doi:10.1055/s-0035-1566739.
16. Hooiveld, M. *et al.* Blood-induced joint-damage: Longterm effects in vitro and in vivo. *J. Rheumatol.* (2003).
17. De Vries-Van Melle, M. L. *et al.* An osteochondral culture model to study mechanisms involved in articular cartilage repair. *Tissue Eng. - Part C Methods* (2012) doi:10.1089/ten.tec.2011.0339.
18. Tekari, A., Egli, R. J., Schmid, V., Justiz, J. & Luginbuehl, R. A Novel Bioreactor System Capable of Simulating the in Vivo Conditions of Synovial Joints. *Tissue Eng. - Part C Methods* (2020)

doi:10.1089/ten.tec.2020.0161.

19. Low, L. A., Mummery, C., Berridge, B. R., Austin, C. P. & Tagle, D. A. Organs-on-chips: into the next decade. *Nature Reviews Drug Discovery* (2021) doi:10.1038/s41573-020-0079-3.

20. Mittal, R. *et al.* Organ-on-chip models: Implications in drug discovery and clinical applications. *J. Cell. Physiol.* **234**, 8352–8380 (2019).

21. Conn, P. M. *Animal Models for the Study of Human Disease*. *Animal Models for the Study of Human Disease* (2013). doi:10.1016/C2011-0-05225-0.

22. Moroni, L. *et al.* Biofabrication: A Guide to Technology and Terminology. *Trends Biotechnol.* **36**, 384–402 (2018).

23. Ali, M. *et al.* A Photo-Crosslinkable Kidney ECM-Derived Bioink Accelerates Renal Tissue Formation. *Adv. Healthc. Mater.* **8**, 1–10 (2019).

24. Ding, X. *et al.* Synthetic peptide hydrogels as 3D scaffolds for tissue engineering. *Adv. Drug Deliv. Rev.* **160**, 78–104 (2020).

25. Saroia, J. *et al.* A review on biocompatibility nature of hydrogels with 3D printing techniques, tissue engineering application and its future prospective. *Bio-Design Manuf.* **1**, 265–279 (2018).

26. Groll, J. *et al.* Biofabrication: Reappraising the definition of an evolving field. *Biofabrication* **8**, (2016).

27. Datta, P., Ayan, B. & Ozbolat, I. T. Bioprinting for vascular and vascularized tissue biofabrication. *Acta Biomater.* **51**, 1–20 (2017).

28. Meinert, C., Schrobback, K., Hutmacher, D. W. & Klein, T. J. A novel bioreactor system for biaxial mechanical loading enhances the properties of tissue-engineered human cartilage. *Sci. Reports 2017 71* **7**, 1–14 (2017).

29. Jeon, J. S. *et al.* Human 3D vascularized organotypic microfluidic assays to study breast cancer cell extravasation. *Proc. Natl. Acad. Sci. U. S. A.* (2015) doi:10.1073/pnas.1417115112.

30. Mansoorifar, A., Gordon, R., Bergan, R. C. & Bertassoni, L. E. Bone-on-a-Chip: Microfluidic Technologies and Microphysiologic Models of Bone Tissue. *Adv. Funct. Mater.* (2021) doi:10.1002/adfm.202006796.

31. Paggi, C. *et al.* Cartilage-on-chip: a multi-modal platform to study human chondrocyte's response to mechanical stimuli. *Osteoarthr. Cartil.* (2020) doi:10.1016/j.joca.2020.02.287.

32. Occhetta, P. *et al.* Hyperphysiological compression of articular cartilage induces an osteoarthritic phenotype in a cartilage-on-a-chip model. *Nat. Biomed. Eng.* (2019) doi:10.1038/s41551-019-0406-3.

33. Lin, H., Lozito, T. P., Alexander, P. G., Gottardi, R. & Tuan, R. S. Stem cell-based microphysiological osteochondral system to model tissue response to interleukin-1B. *Mol. Pharm.* (2014) doi:10.1021/mp500136b.

34. Longoni, A. *et al.* Endochondral Bone Regeneration by Non-autologous Mesenchymal Stem Cells. *Front. Bioeng. Biotechnol.* **8**, 651 (2020).

35. Melchels, F. P. W., Dhert, W. J. A., Hutmacher, D. W. & Malda, J. Development and characterisation of a new bioink for additive tissue manufacturing. *J. Mater. Chem. B* **2**, 2282–2289 (2014).

36. Pouran, B. *et al.* Solute transport at the interface of cartilage and subchondral bone plate: Effect of micro-architecture. *J. Biomech.* (2017) doi:10.1016/j.jbiomech.2016.12.025.

37. Boothe, T. *et al.* A tunable refractive index matching medium for live imaging cells, tissues and model

organisms. *Elife* **6**, (2017).

38. Gong, M. *et al.* Immortalized mesenchymal stem cells: An alternative to primary mesenchymal stem cells in neuronal differentiation and neuroregeneration associated studies. *J. Biomed. Sci.* (2011) doi:10.1186/1423-0127-18-87.

39. Wong, D. Y., Ranganath, T. & Kasko, A. M. Low-Dose, Long-Wave UV Light Does Not Affect Gene Expression of Human Mesenchymal Stem Cells. *PLoS One* **10**, e0139307 (2015).

40. Brauer, A., Pohlemann, T. & Metzger, W. Osteogenic differentiation of immature osteoblasts: Interplay of cell culture media and supplements. *Biotech. Histochem.* (2016) doi:10.3109/10520295.2015.1110254.

41. Bernal, P. N. *et al.* Volumetric Bioprinting of Complex Living-Tissue Constructs within Seconds. *Adv. Mater.* (2019) doi:10.1002/adma.201904209.

42. Gehlen, J., Qiu, W., Müller, R. & Qin, X.-H. Volumetric Tomographic 3D Bioprinting of Heterocellular Bone-like Tissues in Seconds. *bioRxiv* (2021).

43. Naghieh, S., Sarker, M., Izadifar, M. & Chen, X. Dispensing-based bioprinting of mechanically-functional hybrid scaffolds with vessel-like channels for tissue engineering applications – A brief review. *J. Mech. Behav. Biomed. Mater.* **78**, 298–314 (2018).

44. Hamid, O. A., Eltaher, H. M., Sottile, V. & Yang, J. 3D bioprinting of a stem cell-laden, multi-material tubular composite: An approach for spinal cord repair. *Mater. Sci. Eng. C* **120**, (2021).

45. Hauser, P. V. *et al.* Bioprinting Scaffolds for Vascular Tissues and Tissue Vascularization. *Bioeng. (Basel, Switzerland)* **8**, 178 (2021).

46. Hoemann, C. D., Lafantaisie-Favreau, C. H., Lascau-Coman, V., Chen, G. & Guzmán-Morales, J. The cartilage-bone interface. *The journal of knee surgery* (2012) doi:10.1055/s-0032-1319782.

47. Bai, X. *et al.* Self-reinforcing injectable hydrogel with both high water content and mechanical strength for bone repair. *Chem. Eng. J.* **288**, 546–556 (2016).

SUPPLEMENTARY FIGURES

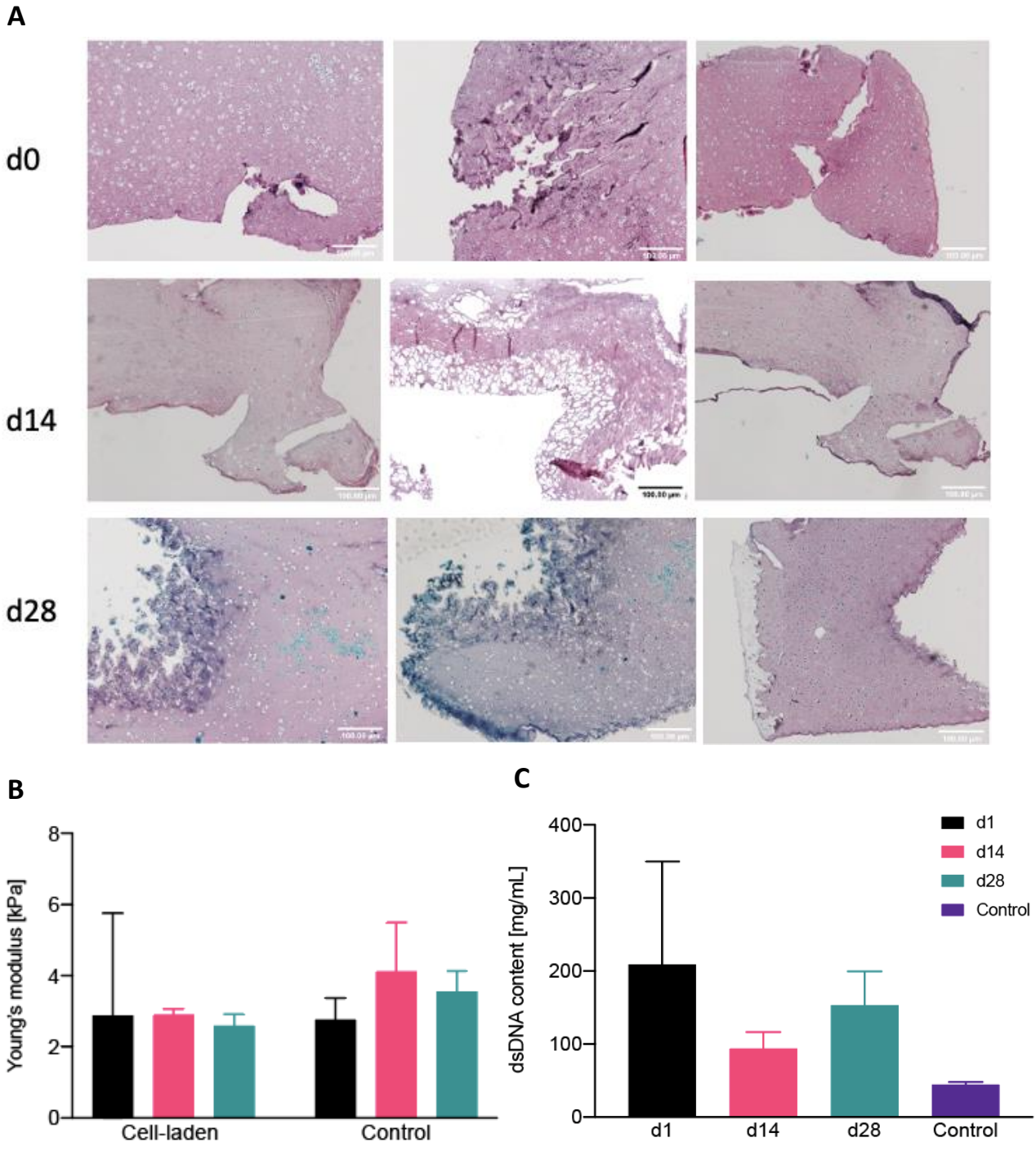

Supplementary figure 1: Cartilage differentiation of 15M ACPC/mL. a) Saffranin O / Fast Green, histology staining for proteoglycans at different time points of differentiation, day 0, day 14 and day 28. Scale bar 100um. b) Young's modulus of the hydrogel samples at different times of collection. Cell-laden samples are ACPC laden hydrogels at days 0, 14 and 28 of culture, controls. c) dsDNA quantification.

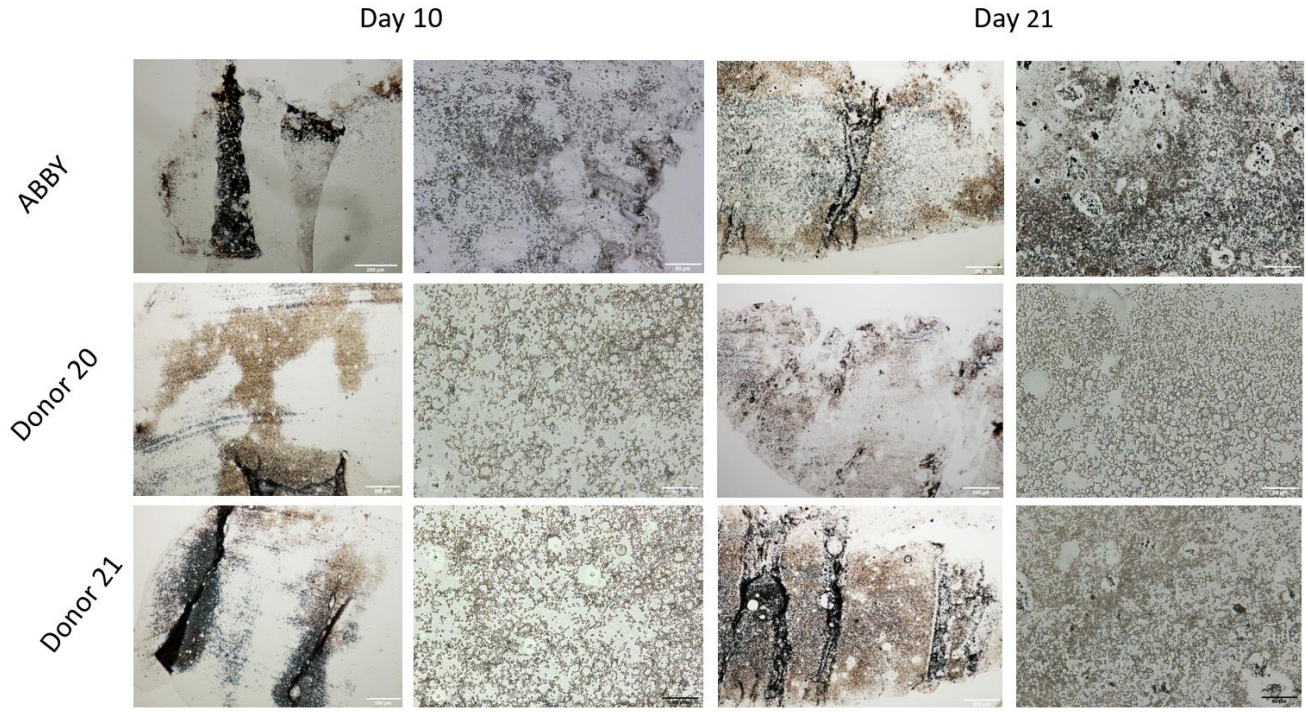

Supplementary figure 2: Bone differentiation of VBP 5M BM-hMSCs/mL of three different BM-hMSC donors. Three BM-hMSC donors were compared for their osteogenic differentiation potential, ABBY, Donor 20 and Donor 21. All images correspond to a Von Kossa staining for Calcium deposits. Pictures in the first and second column correspond to day 10 of bone differentiation while pictures in the third and fourth column correspond to day 21 of differentiation. Scale bars correspond to 100 and 50 µm alternating column one and three, columns two and four.